Capturing the Hardness of Coating Systems Across the Scales

Yilun Xu[1,2], Daniele Dini[2,*]

[1]Department of Materials, Imperial College London, London SW7 2AZ, UK
[2]Department of Mechanical Engineering, Imperial College London, London SW7 2AZ, UK

Abstract

A two-dimensional multi-scale modelling approach that concurrently couples discrete dislocation plasticity and crystal plasticity finite element has been applied to study the hardness variation of coating systems across different scales, covering nano- to micro-indentation. The difference in indentation size sensitivity between film and substrate gives rise to three regimes of hardness, one typically dictated by the intrinsic coating indentation size effect, which is regulated by dislocations activity, and the other two linked to the continuum response of the coating and the substrate. We propose a new hardness formula that incorporates physics-based indentation size effects of thin films into established continuum hardness transition formulae. This formula is shown to substantially improve the hardness prediction of coating systems, particularly when relative indentation depth is at the nanometre scale.

Keywords: dislocation dynamics; hardness; thin films; coating; multi-scale coupling

*Corresponding address: d.dini@imperial.ac.uk.

1 Introduction

Coating systems are extensively employed in industrial applications to reinforce the surface performance of substrate components, for instance mechanical strength, wear resistance, electrical conductivity, etc. The functions of coating systems have been serving industry for several decades; however, understanding the indentation response of crystalline coating systems across the scales remains a challenge to which scientists working in many fields, including *e.g.* materials and tribology, are routinely exposed.

Hardness is one of the key properties [1] used to characterize the response of films and coating systems to interactions with other materials and surfaces. Wear resistance is also strongly linked to the surface hardness [2]. Nanoindentation tests are commonly implemented to determine the hardness of a coating system, whose response strongly depends upon indentation depth. A universally acknowledged rule to exclude the substrate contribution to the coating system is to limit the indentation depth to 10% of the film thickness [3]. The hardness variation is characterised by multiple length scales and one can identify two clear transition regions: one at the film thickness length scale from the film-dominated hardness to the substrate-dominated hardness for relatively large indentation depths [4]; the other manifests itself at the microscopic scale, when applied indentation depth is small compared to the film thickness, and identifies the indentation size effect (ISE) regime [5] before the macroscopic film-dominated hardness is reached (*e.g.* Figure 3). The hardness of coating systems can be as high as three times the continuum value [6-8] within the ISE-dominated region. It is therefore necessary to carefully consider the indentation depth crossing various length scales when the depth-dependent hardness of a composite system is studied.

Most of existing models for predicting coating system hardness are derived from work-of-indentation-based mechanisms [4], which are designed to capture the film-dominated to substrate-

dominated transition. They provide the correlation between a coating system hardness and the relative indentation depth (RID) as:

$$\mathrm{H_c} = \mathrm{H_s} + \frac{\mathrm{H_f} - \mathrm{H_s}}{1 + \kappa_1 \beta^2}, \quad (1)$$

where $\mathrm{H_c}$ is the coating system hardness, $\mathrm{H_s}$ the substrate hardness, $\mathrm{H_f}$ the film hardness, and κ_1 the dimensionless parameter related to indenter geometry and that phenomenologically captures the film-dominated to substrate-dominated transition. In eq. (1), β is the RID, which is defined as the ratio between applied indentation depth and film thickness, viz. $\beta \equiv \delta / h_f$.

Significant efforts have been made to attempt to improve the consistency between numerical prediction and experimental results by modifying eq. (1). Among those, Tuck et al. [9] relaxed the square form of RID, β, to a generalized exponent parameter and hence improved the genericity of the hardness formula. Bull [10] introduced the deformation volume and energy dissipation argument to the indentation-work model, and thus took indentation size effect of films as an additional term in the coating system formula. However, this phenomenological formula did not explicitly detail the dislocation activities within the film and hence lacks physical interpretation of ISE. Tuck et al. [11] proposed a dimensionless parameter for the exponent of RID, β, that was correlated to the indenter geometry and coating system deformation mode. Bull et al. [12] further compared the application of the hardness formula in single and multi-layer hard coating systems. Korsunsky et al. [13] reviewed the work of indentation model and argued that cracking and plasticity could be fully incorporated into the framework by fitting the parameters. Ma et al. [14] performed an important step forward and theirs was the first contribution attempting to provide a full spectrum of composite hardness over a large RID range, covering $\beta = 0.1 - 5$. In particular, they applied the original form of Nix and Gao's formula based on strain gradient theory to incorporate ISE [15] in a continuum model and proposed a modification to the original formula by Korsunsky et al. [4] given in eq. (1).

From the brief overview of this research topic reported above and from screening the many publication dealing with indentation size effects, it is clear that the disparity of scales encountered as the indentation depth is increased, which characterise films and substrates, are not always considered in deriving expressions to estimate or predict hardness variation of coating systems. Attempts that have been made to capture hardness evolution, even when they try to capture transitions at the smallest of scales using mechanisms-based formulations [14], most often are based on a single-scale modelling methods. Furthermore, so far a physics-based modelling approach has not been adopted to reflect the explicit role played by dislocations structures on the ISE of films at the small scales. Capturing such aspect of indentation response is extremely important as it translates into the hypothesis of spherical deformation volume not necessarily being valid [10, 16] and hardness deviation at small indentation depths [14]. Hence, it is essential to develop a multi-scale, physics-based model, which can describe the coating system hardness behaviour over a wide range of length scales. The adoption of a multi-scale model can also provide a better physical interpretation of fitting parameters (such as κ_1 in eq.(1)). In addition, the application of a multi-scale model reduces the computational expense required to study the entire indentation process using simulations methods capable of capturing the smaller scales [17, 18]; these are potentially associated with the need to model large regions of a coating system using microscopically-accurate models, especially when large indentation depths are to be explored [19, 20]. Finally, although atomistic or molecular scale models [21-23] have been recently proposed to study some fundamental aspects on indentation at the smallest of scales, they are too computationally expensive to address issues related to transitions across length-scales and macroscopic hardness.

In this paper, we utilize discrete dislocation plasticity (DDP) as well as a multi-scale modelling approach [18] that couples DDP and crystal plasticity finite element (CPFE) subregions to analyse the indentation response of coating systems typically used in industrial applications. The aim is to capture the indentation behaviour in the ISE region with the accuracy required to study the

microscopic origins of such effect at dislocations level (DDP subregion) while still being able to study the microstructurally-insensitive response at large indentation depths. With the new insight gained from the explicit introduction of dislocations-scale simulations, a new hardness formula, similar to the modified version of eq. (1) proposed in [14] but which adopts an alternative correction for the ISE region, is proposed. The functional form obtained is inspired by the DDP and the multi-scale coupling results and the formula is then used to describe hardness variation of indentation tests on different coating systems. The effectiveness of the newly proposed formula in capturing the hardness variations for different systems and over a large range of indentation depths demonstrates its suitability for incorporation in design methodologies for coating systems.

2 Methodology

First, studies are carried out to simulate indentation of thin coating films using DDP and CPFE individually to show how the two methodologies describe coatings indentation processes and to evaluate their hardness response. After the initial studies have been conducted using individual modelling tools suitable to capture the behaviour at different time and length scales to highlight their strengths and potential limitations, a concurrent multi-scale model that couples DDP and CPFE formulations is applied to the coating systems under investigation to study the transition between ISE and the size-independent response of the coating as well as the effect of the substrate on the system response to indentation to overcome the issue encountered with the separate descriptions.

2.1 DDP and CPFE formulations

A planar, isotropic and isothermal DDP framework [18] is adopted to investigate the indentation size dependence of film behaviour under nanoindentation. Even though the 2D representation of this DDP methodology has its limitations in terms of generality and universal applicability, it is an extremely useful tool to provide localized information at the dislocation scale during plastic deformation and has been widely applied to indentations of thin films. The plastic flow within the

thin film results from the collective motion of dislocations gliding along predefined slip planes. There are three predefined slip systems in the DDP model oriented by $\phi^{(s)} = \pm 35.3, 90, s = 1, 2, 3$ with respect to the y-axis, which represents the activated systems in a typical FCC crystal. The linear superimposition scheme proposed in [24] is adopted herein to solve the boundary problem. The total displacement field $\boldsymbol{u}$ is decomposed into a $\widetilde{\boldsymbol{u}}$ field, which sums the displacement field contribution of dislocations, and an image field $\widehat{\boldsymbol{u}}$, which corrects the boundary conditions. The total stress $\boldsymbol{\sigma}$ and strain $\boldsymbol{\epsilon}$ fields are analogously obtained by superimposition of the image field ($\widehat{\ }$) and the sum of individual dislocation field ($\widetilde{\ }$) as:

$$\begin{aligned} \boldsymbol{u} &= \widetilde{\boldsymbol{u}} + \widehat{\boldsymbol{u}} \\ \boldsymbol{\sigma} &= \widetilde{\boldsymbol{\sigma}} + \widehat{\boldsymbol{\sigma}} \\ \boldsymbol{\epsilon} &= \tilde{\boldsymbol{\epsilon}} + \hat{\boldsymbol{\epsilon}} \end{aligned} \tag{2}$$

Dislocations activities follow a series of governing laws, including nucleation, mobility, pinning, etc., but thermal effects on dislocations activities [25] are neglected. The rate-sensitivity of the DDP framework mainly comes from the mobility law [26], and diminishes when a relatively high strain rate is imposed on the sample. Details about the DDP numerical framework and simulation set-up of the nanoindentation are provided in [18] and [27], respectively. A rate-independent CPFE formulation [28], where the slip along slip systems occurs is dominated by thermal-activation process [29], is adopted either to model the response of the coating and the substrate at the continuum level or to study the size-independent region response in the coupled simulations described below. The key formulations in the CPFE framework are concisely summarized herein, and more details can be found in Ref. [29] . The plastic velocity gradient $\boldsymbol{L^p}$ sums up the slip rate $\dot{\gamma}^{(i)}$ along all active slip systems, which gives:

$$\boldsymbol{L^p} = \sum_{i=1}^{M} \dot{\gamma}^{(i)} \boldsymbol{s}^{(i)} \otimes \boldsymbol{n}^{(i)} \tag{3}$$

here M is the total number of slip systems ($M = 12$ for an FCC crystal), $\boldsymbol{s}^{(i)}$ and $\boldsymbol{n}^{(i)}$ are the slip direction and normal direction vector of i^{th} slip system, respectively. The slip rate $\dot{\gamma}^{(i)}$ along i^{th} slip system is constitutively governed by thermally activated dislocation escaping from obstacles (such as lattice defect, impurities, inclusions, etc), which is given by:

$$\dot{\gamma}^{(i)} = \rho_{ssdm} b^2 v_D \exp\left(-\frac{\Delta H}{k\theta}\right) \sinh\left(\frac{\Delta V}{k\theta}\left|\tau^{(i)} - \tau_c^{(i)}\right|\right) \tag{4}$$

where $\rho_{ssdm}$is the initial mobile statistically stored dislocation density, b is the Burgers vector, v_D the dislocation jump frequency, ΔH is the activation energy, k is the Boltzmann constant, ΔV is the activation volume, $\tau^{(i)}$ and $\tau_c^{(i)}$ are the resolved shear stress and critical resolved shear stress on i^{th} slip system, respectively. The critical resolved shear stress $\tau_c^{(i)}$ increases with increased dislocation density. An appropriate combination of ΔH and ΔV effectively suppresses the rate sensitivity of the plasticity and macroscopic material response within a certain strain-rate range [30].

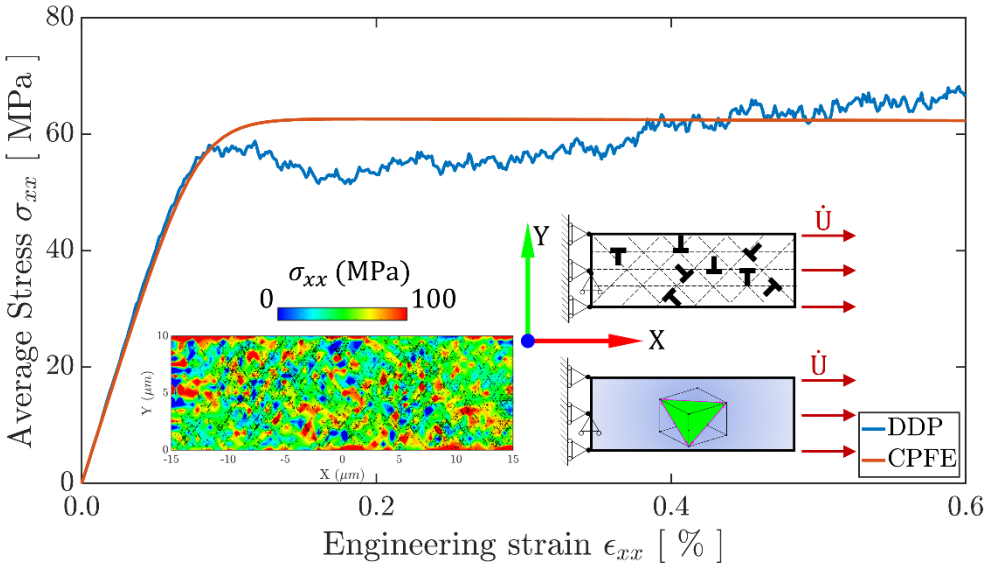

Figure 1. stress strain response curve of DDP and CPFE single crystal under uniaxial loading. CPFE material properties are calibrated to match the DDP stress response, and stress field of the DDP single crystal is illustrated with corresponding dislocation structure when $\epsilon_{xx} = 0.6\%$.

2.2 Multi-scale coupling framework between DDP and CPFE

The DDP parameters for modelling the thin films behaviour are chosen as to represent material behaviour for an aluminium-like single FCC crystal as shown in [31]. CPFE parameters are calibrated

to the corresponding stress-strain response of the DDP model under uniaxial tension as shown in Figure 1. The calibrated CPFE and DDP parameters are tabulated in Table 1, and further details can be found in Xu et al. [18]. The adopted activation energy and volume are in line with those reported in the literature [32, 33] and the combination of their values corresponds to a very low rate sensitivity of the thin films.

In the coupled simulations the ISE-dominated film sub-region is modelled using DDP and the remaining part of the sample is modelled using CPFE. The multi-scale coating system with two sub-regions is sketched in Figure 2(a). The indentation process is divided into several time steps; at each load increment, the film subregion (Ω_{DDP}) receives boundary conditions from the indenter and previous CPFE calculations, and outputs traction via nodes along the coupling interface (Γ_{DDP}). The substrate sub-region (Ω_{CPFE}) inputs tractions received from Ω_{DDP} and feedbacks displacement field via the coupling interface (Γ_{CPFE}) for the next DDP calculation.

Table 1. Material properties in DDP and CPFE modelling

Subregion	Parameter Name	Symbol	Unit	Value
Both	Young's modules	E	GPa	70
	Poisson ratio	υ	-	0.33
	Burger's vector	b	nm	0.25
DD	Spacing of slip planes	-	b	100
	Drag coefficient	B	$\mathrm{Pa \cdot s}$	10^{-4}
	Annihilation distance	L_e	b	6
	Mean source strength	$\bar{\tau}_{nuc}$	MPa	50
	Obstacle strength	τ_{obs}	MPa	150
	Source density	ρ_{nuc}	μm^{-2}	40
	Obstacle density	ρ_{obs}	μm^{-2}	80
	Critical resolved shear stress	τ_{CRSS}	MPa	12
CP	Hardening coefficient	λ	μm^{-2}	2.0
	Mobile dislocation density	ρ_{ssdm}	μm^{-2}	1.2
	Activation energy	ΔH	$\mathrm{kJ \cdot mol^{-1}}$	110
	Activation volume	ΔV	–	$50\mathrm{b}^3$

An iterative scheme (illustrated in Figure 2(b)) is adopted to achieve both traction and displacement compatibility at the coupling interface the film and substrate [34, 35]. The indentation boundary

condition updates until convergence is achieved at the current indentation depth. More specifically, the DDP subregion outputs the stress field to the CPFE subregion via the interface boundary, and the CPFE subregion uses this to enforce new traction boundary conditions for its advancement. Then the CPFE subregion passes its displacement field back to the DDP subregion such that the latter can start iterating the calculation with the updated boundary conditions until equilibrium and consistency are enforced throughout the sample.

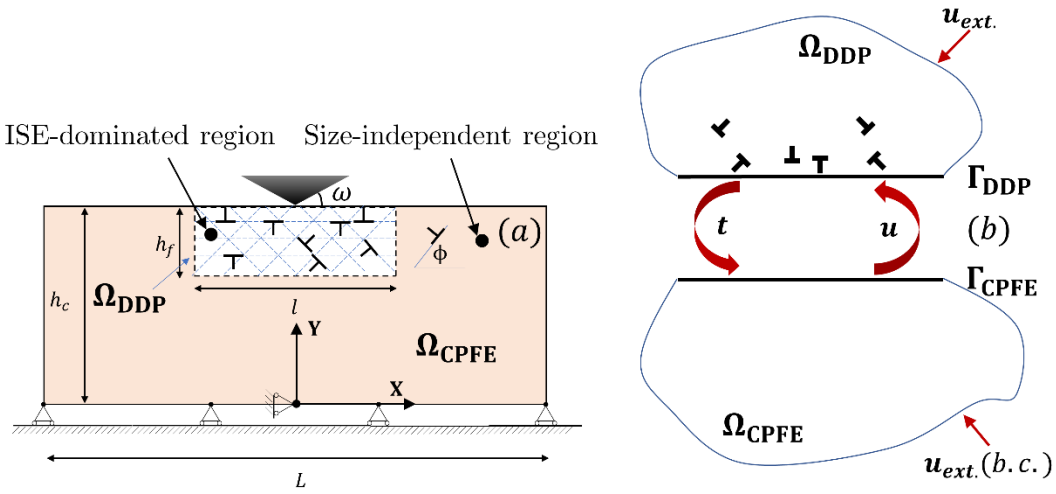

Figure 2. (a) Schematic diagram of the multi-scale coating system containing two subregions under wedge-shaped indentation (b) Traction and displacement exchange via coupling interface between DDP and CPFE sub-regions.

The coupling interface between the DDP and CPFE subregions is modelled transparent to dislocation transmission [34]. The dislocations approaching the coupling interface (the critical distance is set as 100b in this study) are removed from the DDP subregion, but the stress field introduced by those dislocations is fully transferred by utilizing the iterative scheme (Figure 2(b)) between the DDP and CPFE subregion. Therefore, the incompatibility between DDP and CPFE subregions' fields due to the singularity of individual dislocations no longer hinders the concurrent coupling approach. The methodology and algorithm describing the "quasi-transfer" of dislocation's flux from the DDP subregion to the CPFE subregion (*i.e.* the CPFE subregion absorbs dislocations via field exchange) is detailed in [34]. The singularity due to the dislocations near the coupling interface is hence resolved without losing information from the dislocation scale to the crystal scale. Alternative schemes can

also be easily implemented within the coupling framework to include effects such as the presence of grain boundaries (e.g. modelling dislocation pile-ups) and discontinuities between the DDP and CPFE regions. For a more detailed description of the iterative scheme and multi-scale coupling methodology is referred to Xu et al. [18].

3 Numerical Results and New Hardness Formula

3.1. Discrete Dislocation Plasticity Simulations

We start by focusing on a discrete dislocation plasticity analysis (*i.e.* without coupling to the crystal plasticity substrate), which was conducted on two films of thickness $h_{DD} = 2\mu\text{m}$ and $h_{DD} = 10\mu\text{m}$ indented by a wedge-shaped indenter with $\omega = 5°$ to show the level of details achieved with such simulations. The simulations were performed with the thin films bonded to a rigid substrate *i.e.* the degree of freedoms along the bottom surfaces are constrained. While highlighting the physical insight that these simulations can produce, we also look at the main limitations of the method, which is that it can only be used to study the behaviour of the film for limited indentation depths compared to the sample thickness – note that a rigid substrate bonded to the thin film is conventionally assumed rather that explicitly modelling the presence of the substrate and its characteristics explicitly due to the expense involved with explicitly modelling the dislocation activity within the substrate and across the boundary. The indentation pressure response (commonly referred to as hardness in this context), which is calculated as the ratio between the reaction force and the contact size, as a function of the applied indentation depth is reported in Figure 3 for both films.

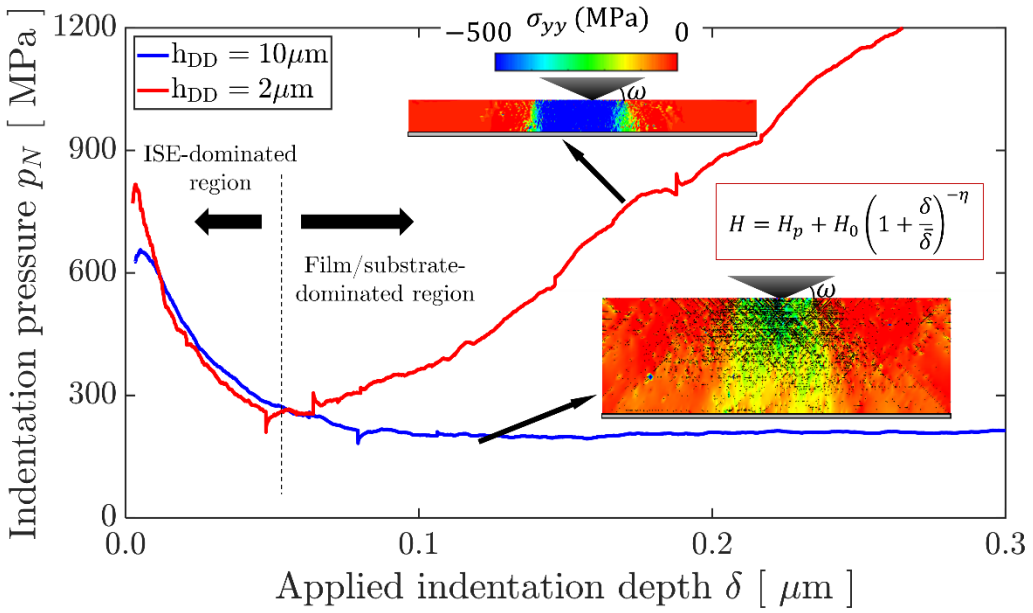

Figure 3. Indentation pressure response as a function of the applied indentation depth of two films with different thickness modelled using discrete dislocation plasticity.

When indentation depth is small ($\delta < 0.06\mu m$), the indentation pressure decreases with applied indentation depth, and the trend appears similar for the two film. The discrepancy at extremely small indentation depths is caused by the mesh sensitivity of contact resolution [36]. However, indentation pressure increases for the thin film when plastic flow reaches the rigid boundary (compressive stress through the film shown in the contour plot), which is given by dislocations approaching and piling up at the bottom boundary; this causes significant back forces are developed when the indentation depth exceeds 10% film thickness.

It is worth noticing that the presence of the substrate is already felt at a smaller level of RID ($\delta = 0.3\mu m, \beta = 3\%$) compared to the conventional continuum estimation ($\beta = 10\%$) for thin films [3]. This is attributed to discrete nature of dislocation movement towards the rigid boundary that triggers the substrate effect sooner than continuum plastic flow. For the thick film, its indentation pressure continues to decay until an indentation size independent plateau ($p_N \approx 218\text{MPa}$) is achieved. In this case, the stress field contour shows that the plastic flow introduced by collective dislocation glide is still far from the rigid boundary at indentation depth $\delta = 0.3\mu m$ (note that the contours are plotted at the same indentation depth for both films). These simulations allow to

capture the variation of indentation pressure within ISE regime in thick films (without considering the effect of the rigid substrate), which has been quantitatively investigated using DDP analysis [27] , and is given by a modified form of Nix and Gao's formula [15]:

$$\mathrm{H} = \mathrm{H_p} + \mathrm{H_0}\left(1 + \frac{\delta}{\bar{\delta}}\right)^{-\eta}, \tag{5}$$

where $\mathrm{H_p}$ is the size-independent continuum hardness, $\mathrm{H_0}$ the initial hardness, $\bar{\delta}$ the length scale parameter associated with dislocation source spacing, and η a power-law exponent usually in the range between 0.5 and 0.7 [27].

3.2. CPFE and Coupled Simulations

Analogous calculations were performed using CPFE only (shown in Figure 1 for the larger of the two domains). The film hardness is predicted by the CPFE to be $165\mathrm{MPa}$, close to three times the flow stress for this specific material, as expected from classical macroscopic plasticity arguments [37], and does not exhibit an indentation size dependent regime. Note therefore that there is a difference between the DDP computed hardness ($218\mathrm{MPa}$, denoted by the dashed red line, Figure 4 – not reported in legend as not obtained directly by simulations but estimated using the DDP-only results) and the continuum equivalent value ($165\mathrm{MPa}$, denoted by the dashed green line, Figure 4). This is likely due to the fact that, although the two descriptions have been calibrated under uniaxial tension, some differences emerge when the state of stress is multiaxial and the DDP response is computed in an inhomogeneous system.

The indentation pressure response of the multi-scale coating system ($h_c = 10\mu\mathrm{m}$) against relative indentation depth is reported in Figure 4. Here Ω_{DDP} corresponds to the film domain were most of the dislocation activity is concentrating (top, $h_{DD,coupling} = 2\mu\mathrm{m}$) and Ω_{CPFE} is used to model the remaining part of the film region, away from where the indentation size effect is captured.

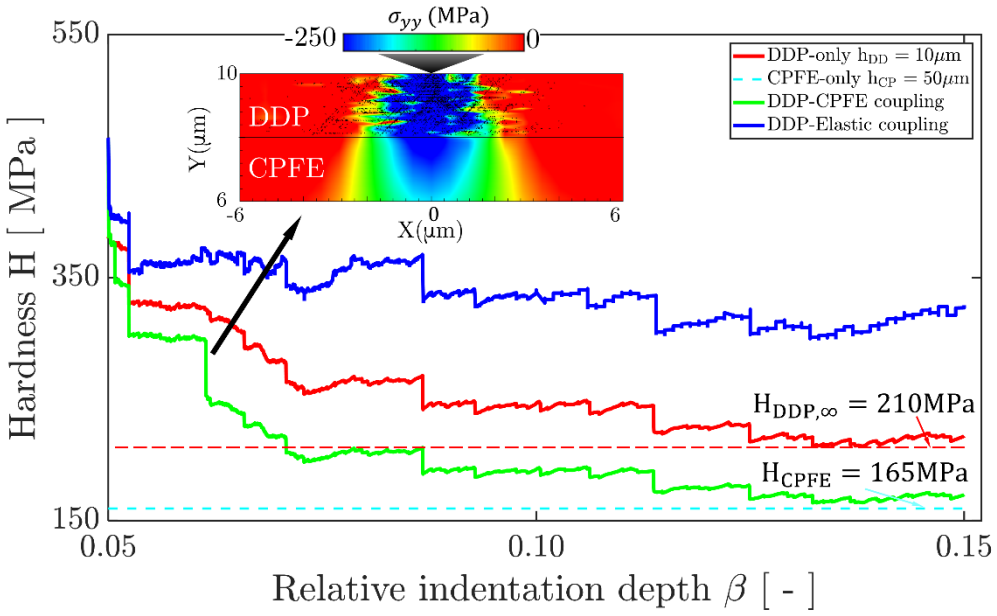

Figure 4. A comparison between the indentation pressure response of the multi-scale coating system, the film modelled using DDP only ($h_{DD} = 10\mu m$), the full system modelled using CPFE only ($h_{CP} = 50\mu m$). The stress field of the multi-scale coating system is illustrated in the inset of the figure also to highlight traction compatibility achieved at the coupling interface. The hardness response of a DDP-Elastic coating system is also included to demonstrate the necessity of assigning the CPFE material properties to the substrate subregion to correctly capture the system behaviour.

Therefore, given the hardness values reported above for the separate materials' description, this sample corresponds to a coating system characterised by a coating slightly harder than the substrate. The indentation pressure response of the DDP film of thickness $h_{DD} = 10\mu m$ and the results obtained using CPFE in a large domain, $h_{CP} = 50\mu m$, are also included. The hardness evolution of the coating system shows a typical indentation size effect regime and is dominated by DDP film behaviour when relative indentation depth is small, i.e. $\beta < 10\%$. However, the presence of the CPFE substrate is felt when the indenter penetrates further into the film. Even for a film of thickness $10\mu m$ there is a tangible difference between the film analysed used DDP-only and the results obtained through the coupling scheme, as the multi-scale DDP-CPFE model produces a softer response; this is likely due to the fact that the DDP and the CPFE descriptions have been matched with a calibration aimed at capturing the macroscopic response of the material under uniaxial tension rather than the local response; this is bound to cause discrepancies when the two descriptions are used to capture important strain gradients localised underneath the indenter tip.

Nevertheless, the coupling scheme ensures that the transition to the macroscopic response of the coating is captured.

An additional multi-scale coupling simulation, which replaces the CPFE subregion in Figure 2 with the corresponding anisotropy elastic material (*i.e.* by setting the CRSS value to infinity) was also conducted, the hardness response of which is represented by the blue curve in Figure 4. As expected, the use of the elastic substrate substantially overestimates the hardness the coating system when the indenter feels the substrate, $\beta > 5\%$; this is due to the large equivalent stiffness of the elastic substrate compared to the more compliant response of the CPFE, which allows to better accommodate deformations and the development of plastic strains within the material. This further demonstrates that an accurately calibrated CPFE substrate is essential for representing the multi-scale coating system.

3.3. Proposed Hardness Formula to Capture the Behaviour across the Scales

Our previous study [27] on the dependence of the hardness response of thin films on dislocation structures has provided a microstructure-dependent hardness formula that should be applied when the indentation depth is relatively small compared to the film thickness. The multi-scale coupling results shown in Figure 4 suggests that the hardness transition between the DDP domain (which can be used to describe the behaviour of the thin coating) and the CPFE domain (which can be used to model the substrate or the region far from the large strain gradients near the indenter tip for relatively thick coatings) has been captured by the hybrid modelling method. The scheme can be used to explore the subtleties of the transition between film and substrate and to correctly mimic the hardness variation of a coating system across the scales. By incorporating the recent DDP analysis of the film response in the ISE and the concurrent multi-scale coupling results in the conventional descriptions of hardness for thin films, we propose a new hardness formula for a coating system, which simultaneously captures both the indentation size effect regime and the hardness transition

regime from film to substrate. The continuum-based formula (eq.(1)) proposed by Korsunsky and co-workers [9, 38] is used as our starting point; however, the invariant film hardness is replaced by the indentation size dependent formula that capture the transition between ISE-dominated and film-dominated region (eq. (5)), which gives:

$$H_c = H_s + \frac{H_{f,p} + H_{f,0}(1 + \frac{\beta}{\bar{\beta}})^{-\eta} - H_s}{1 + \kappa_2 \beta^2} \quad (6)$$

where H_c is the size-dependent hardness of the coating system, $H_{f,p}$ the size-independent hardness of the film, $H_{f,0}$ the initial hardness of the film, which can be determined from material elasticity and indenter geometry [39], $\bar{\beta}$ the relative length scale parameter, H_s the continuum hardness of substrate, and κ_2 the modified dimensionless hardness transition parameter. The relative length scale parameter $\bar{\beta}$ is the same as the length scale parameter $\bar{\delta}$ in eq.(5) (the nomenclature has been adapted here so that the parameter can be directly related to the RID , β), and captures the hardness reduction within the indentation size effect regime. The magnitude of the length scale parameter $\bar{\beta}$ has been correlated to the dislocation spacing of the materials under investigation [27], which in turn can be linked to manufacturing processes, residual strain, etc.

It should be noted here that although the proposed formula in eq. (6) resembles the correction proposed by Ma et al. [14], its nature and derivation stems from a different perspective. In this paper we make use of the explicit knowledge obtained using DDP simulations and the new insight provided by looking at the influence of dislocations structures on ISE [27] to provide a different interpretation of the correction obtained by Ma et al. [14] using more conventional strain-gradient plasticity predictions. The newly proposed formula therefore fully incorporates its physics-based ingredients, in the order of length scales, as follows: (a) the depth-sensitive hardness variation (*i.e.* indentation size effect) of the film predicted using the improved understanding obtained using DDP [27] ; (b) the continuum hardness transition between the film and the substrate provided by the work-of-

indentation-based mechanisms [4] ; (c) the depth-insensitive, continuum hardness of the substrate that is physically governed by its flow stress [37].

The difference between the two descriptions of the hardness response as function on indentation depth provided by eqs. (1) and (6) is schematically depicted in Figure 5. Here it is emphasised how the newly proposed formula provides the necessary means to include the contribution of the ISE for very small indentation depths. This could then potentially used to interpret and predict the behaviour of different coating materials and substrates across the scales.

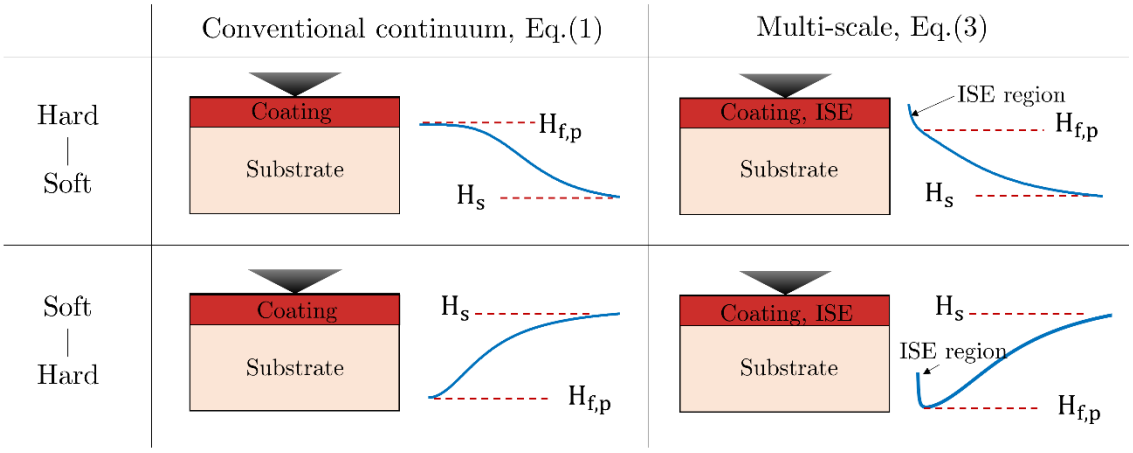

Figure 5. Schematic representation of the response of different coating systems provided by the classical continuum-based transition formula and the newly proposed formula to predict hardness variation in thin films as a function of indentation depth.

4 Discussion

Experimental results are now used to show how the new formula can be used to provide a better description of the indentation process of thin coating films. Comparison of the fitting for nanoindentation experimental data obtained for two different coating systems using the conventional continuum formula, eq.(1), and the proposed multi-scale formula, eq.(6), is shown Figure 6. Figure 6(a) illustrates the hardness variation of a nickel ($H_{f,p} = 2.26\text{GPa}$ and $H_{f,0} = 5.70\text{GPa}$) / copper ($H_s = 0.29\text{GPa}$) coating system recorded through nanoindentation tests [9]. This represents a typical hard-soft combination of film and substrate used extensively for industrial applications. Compared to the fitting obtained using eq.(1), eq.(6) substantially improves the fitting

quality, especially in the ISE-dominated region of nanoindentation and provides better prediction within the whole span of relative indentation depth. Figure 6(b) illustrates the hardness variation of an aluminium ($H_{f,p} = 0.45\text{GPa}$, $H_{f,0} = 2.5\text{GPa}$) / glass ($H_s = 6.8\text{GPa}$) coating system [14], which represents a soft-hard combination encountered in various applications. The hardness of the coating system initially decreases to the size-independent hardness of the film and then increases when the influence of the stiffer substrate affects the system behaviour. The newly proposed formula is capable of predicting these two transitions effectively, especially when the indentation size is small. By contrast, the conventional formula eq.(1) can only fit the hardness of a coating system well when the indentation depth is large. It should be noted here that the modified continuum model proposed in [14], in spite of representing the general trend of hardness variation within a relatively large range of relative indentation depths, fails to capture the transition in the ISE-dominated region. Furthermore, the parameter that captures the transition between the film and substrate dominated regions (κ_2) may be strongly affected by the coupling between the scales, *i.e.* in case the films are extremely thin and the two transitions (identified by $\bar{\beta}$ and κ_2 respectively) are relatively close; this is certainly the case in Figure 6(b), where any form of fitting other than eq.(6) would fail to capture the correct hardness variation. In general, this implies that the values obtained for κ_2 and κ_1 may also differ. The exponent fitting parameter η can be fixed within a narrow range as shown with DDP analyses in our previous contribution [40]. The fitting parameters obtained using both equations for the two types of coating systems are tabulated in Table 2.

Table 2. Fitting parameters using eq.(1) and eq.(6) for the two coating systems

Film/substrate	$\boldsymbol{\kappa_1}$	$\boldsymbol{\kappa_2}$	$\bar{\boldsymbol{\beta}}$	$\boldsymbol{\eta}$
Ni/Cu	24	20	0.0007	0.68
Al/glass	0.05	0.04	0.0045	0.65

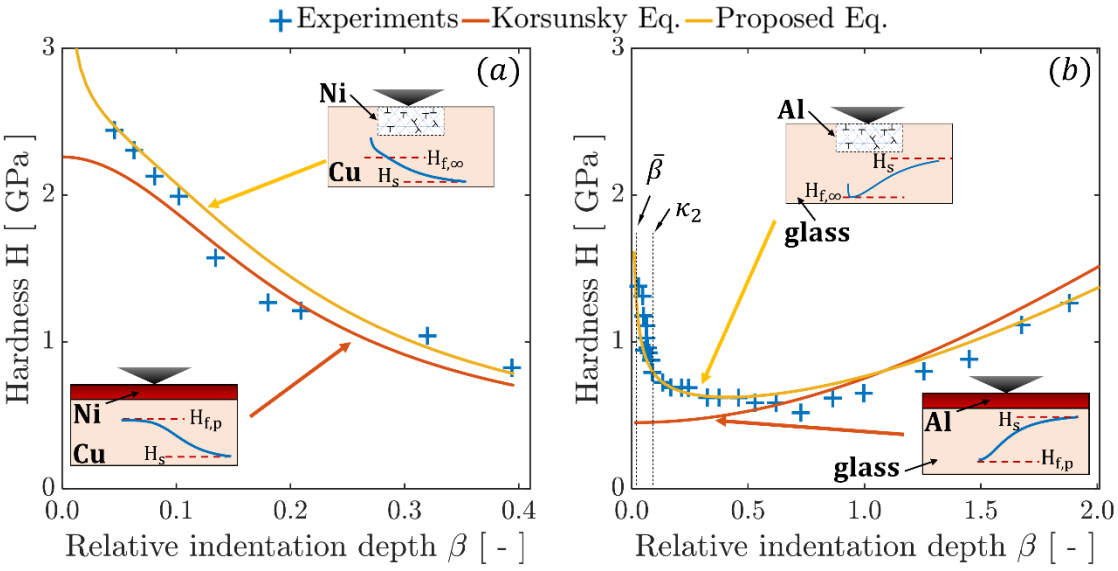

Figure 6. Comparison between fitting experimental data ([9, 14]) of nanoindentation on two coating systems composed of (a) nickel-copper (b) aluminium-glass using eq.(1) and eq.(6), respectively.

Although the constitutive law and formula proposed by Ma et al. [14] generally was shown to match the hardness variation of a number of coating systems well, the use of the original form of Nix and Gao's formula to qualitatively capture the behaviour in the ISE region, which has been shown to leads to discrepancies in predicting hardness at small indentation depths [41, 42]. Furthermore, the numerical model used in Ma et al. [14] to study the transitions of hardness response across the scales is still based on the continuum finite element calculations, and it relies on strain-gradient theory rather than the analysis of dislocation-scale deformations, particularly the stress field due to dislocation activities [43, 44] near the indenter tip. It should be noted that the individual terms provided in the formula proposed in this paper can all be linked to the physical interpretation of response to indentation and terms governing different length scales are also linked to relevant materials length scales as proposed in Ref. [27].

The multi-scale coupling between the DDP and CPFE subregions has not only acted as an inspiration for the development of the new formula (eq.(6)), especially in the effort to study the dislocation-mediated response over large regions of material, but has also provided the tools to enable the physical interpretation of the hardness transitions between the regions controlled by dislocation

structures (ISE-dominated) and between the coating film and the substrate with the support of explicit outputs in terms of dislocations, plasticity and dislocation-mediated stress distributions. (as shown in the inset Figure 4). The use of the different simulations tools provides us with an opportunity to clarify the different mechanisms taking place at different scales and gives the reader the reasoning behind the physical interpretation not only of the formula but also of the transition parameters (e.g. κ_1 in eq.(1)), which is key for enabling researchers (and industries developing new materials and coatings) with the understanding needed and the prediction capabilities to produce new innovative solutions. Furthermore, the use of the concurrent coupling between DDP and CPFE has the potential to provide detailed information about the deformation process that cannot be obtained by the two descriptions in isolation and has enabled us to shed light into the correlation between the microstructure and hardness variation and to show when such transitions take place as a function of the indentation depth.

5 Conclusion

Many attempts of using single-scale models to study coating systems (including those reviewed here and many others, *e.g.* [45, 46]) have hardly shown to be capable of capturing the hardness response of coating systems across the scales. Better predictive capabilities have been shown in this respect by embedding strain-gradient theory into a continuum description to capture the materials behaviour in the ISE-dominated region [14]. Here, inspired by the use of a multi-scale model that couples DDP and CPFE to track the detailed material deformation (especially the details of deformation given by the discrete nature of dislocations within the DDP subregion) and hardness transitions during indentation process, we have taken this one step further. Thanks to the insight gained from the study of the effect that dislocation structure have on the ISE, a modified form [27] of Nix and Gao's formula has been used to propose a new hardness/indentation depth formula. This resolves the issues encountered in the past to capture thin films behaviour in size-sensitive regions

and hence improves the hardness prediction for coating systems. Moreover, the length scale parameter $\bar{\beta}$ in eq.(6) has also been shown to be linked to dislocation source spacing, and therefore provides a physics-based interpretation of how microstructural changes induced by e.g. heat treatments may affect the ISE regime and the overall thin film indentation response.

To conclude, the proposed formula substantially improves the capability to capture size-dependent hardness variation with indentation depth for various coating systems; its use and physical interpretation of the parameters used to describe the transitions of the response across the scales and to match experimental data enables the design of new materials, treatments and solutions to improve coating system performance.

Acknowledgements

This work was supported by the Engineering and Physical Sciences Research Council (EPSRC) [Reference: EP/N025954/1].

References

[1] B.W. Mott, Micro-indentation hardness testing, Butterworths Scientific Publications, 1956.
[2] K. Krishnaveni, T.S.N.S. Narayanan, S.K. Seshadri, Surf Coat Tech, 190 (2005) 115-121. DOI: 10.1016/j.surfcoat.2004.01.038
[3] W.C. Oliver, G.M. Pharr, J Mater Res, 7 (1992) 1564-1583.Doi 10.1557/Jmr.1992.1564
[4] A.M. Korsunsky, M.R. McGurk, S.J. Bull, T.F. Page, Surf Coat Tech, 99 (1998) 171-183. DOI: 10.1016/S0257-8972(97)00522-7
[5] K. McElhaney, J. Vlassak, W. Nix, J Mater Res, 13 (1998) 1300-1306
[6] B. Liu, X. Qiu, Y. Huang, K.C. Hwang, M. Li, C. Liu, J Mech Phys Solids, 51 (2003) 1171-1187.https://doi.org/10.1016/S0022-5096(03)00037-1
[7] B. Liu, Y. Huang, M. Li, K.C. Hwang, C. Liu, Int J Plasticity, 21 (2005) 2107-2122.https://doi.org/10.1016/j.ijplas.2005.03.016
[8] Y. Liu, S. Varghese, J. Ma, M. Yoshino, H. Lu, R. Komanduri, International Journal of Plasticity, 24 (2008) 1990-2015.https://doi.org/10.1016/j.ijplas.2008.02.009
[9] J.R. Tuck, A.M. Korsunsky, R.I. Davidson, S.J. Bull, D.M. Elliott, Surf Coat Tech, 127 (2000) 1-8. DOI: 10.1016/S0257-8972(00)00537-5
[10] S.J. Bull, Thin Solid Films, 398 (2001) 291-298.Doi 10.1016/S0040-6090(01)01374-8
[11] J.R. Tuck, A.M. Korsunsky, D.G. Bhat, S.J. Bull, Surface and Coatings Technology, 139 (2001) 63-74. DOI: 10.1016/s0257-8972(00)01116-6
[12] S.J. Bull, D.G. Bhat, M.H. Staia, Surf Coat Tech, 163 (2003) 499-506.Pii S0257-8972(02)00650-3. DOI: 10.1016/S0257-8972(02)00650-3
[13] A.M. Korsunsky, A. Constantinescu, Materials Science and Engineering: A, 423 (2006) 28-35.https://doi.org/10.1016/j.msea.2005.09.126
[14] Z.S. Ma, Y.C. Zhou, S.G. Long, C. Lu, International Journal of Plasticity, 34 (2012) 1-11. DOI: 10.1016/j.ijplas.2012.01.001
[15] W.D. Nix, H.J. Gao, J Mech Phys Solids, 46 (1998) 411-425. DOI: 10.1016/S0022-5096(97)00086-0
[16] B.D. Fabes, W.C. Oliver, R.A. Mckee, F.J. Walker, J Mater Res, 7 (1992) 3056-3064. DOI: 10.1557/Jmr.1992.3056
[17] N. Shankha, J. Till, C. William, Model Simul Mater Sc, (2019)
[18] Y. Xu, D.S. Balint, D. Dini, Model Simul Mater Sc, 24 (2016) 045007.Artn 045007. DOI: 10.1088/0965-0393/24/4/045007
[19] A. Widjaja, E. Van der Giessen, A. Needleman, Acta Mater, 55 (2007) 6408-6415. DOI: 10.1016/j.actamat.2007.07.053
[20] D. Saraev, R.E. Miller, Acta Materialia, 54 (2006) 33-45. DOI: 10.1016/j.actamat.2005.08.030
[21] R.E. Miller, L.E. Shilkrot, W.A. Curtin, Acta Mater, 52 (2004) 271-284. DOI: 10.1016/j.actamat.2003.09.011
[22] A.K. Nair, E. Parker, P. Gaudreau, D. Farkas, R.D. Kriz, Int J Plasticity, 24 (2008) 2016-2031.https://doi.org/10.1016/j.ijplas.2008.01.007
[23] W.C.D. Cheong, L.C. Zhang, Nanotechnology, 11 (2000) 173-180. DOI: 10.1088/0957-4484/11/3/307
[24] E. Van der Giessen, A. Needleman, Model Simul Mater Sc, 3 (1995) 689-735
[25] Y. Xu, K. Fox, D. Rugg, F.P.E. Dunne, International Journal of Plasticity, (2020) 102753.https://doi.org/10.1016/j.ijplas.2020.102753
[26] Z.B. Zheng, D.S. Balint, F.P.E. Dunne, Acta Materialia, 107 (2016) 17-26. DOI: 10.1016/j.actamat.2016.01.035
[27] Y. Xu, D.S. Balint, D. Dini, Surf Coat Tech, 374 (2019) 763-773.10.1016/j.surfcoat.2019.06.045
[28] A. Manonukul, F.P.E. Dunne, P R Soc A, 460 (2004) 1881-1903. DOI: 10.1098/rspa.2003.1258

[29] F.P.E. Dunne, D. Rugg, A. Walker, International Journal of Plasticity, 23 (2007) 1061-1083. DOI: 10.1016/j.ijplas.2006.10.013
[30] N.G. Prastiti, Y. Xu, D.S. Balint, F.P.E. Dunne, International Journal of Plasticity, (2019).https://doi.org/10.1016/j.ijplas.2019.10.003
[31] D.S. Balint, V.S. Deshpande, A. Needleman, E. Van der Giessen, Model Simul Mater Sc, 14 (2006) 409-422.10.1088/0965-0393/14/3/005
[32] F. Diologent, R. Goodall, A. Mortensen, Acta Mater, 59 (2011) 6869-6879.https://doi.org/10.1016/j.actamat.2011.07.021
[33] D. Ovono Ovono, I. Guillot, D. Massinon, Journal of Alloys and Compounds, 432 (2007) 241-246. https://doi.org/10.1016/j.jallcom.2006.05.132
[34] M. Wallin, W. Curtin, M. Ristinmaa, A. Needleman, Journal of the Mechanics and Physics of Solids, 56 (2008) 3167-3180. DOI: 10.1016/j.jmps.2008.08.004
[35] M.D. Sangid, T. Ezaz, H. Sehitoglu, I.M. Robertson, Acta Materialia, 59 (2011) 283-296. DOI: 10.1016/j.actamat.2010.09.032
[36] A. Widjaja, E. Van der Giessen, V.S. Deshpande, A. Needleman, J Mater Res, 22 (2007) 655-663. DOI: 10.1557/Jmr.2007.0090
[37] J.R. Cahoon, W.H. Broughton, A.R. Kutzak, Metallurgical Transactions, 2 (1971) 1979-1983. DOI: 10.1007/BF02913433
[38] A.M. Korsunsky, A. Constantinescu, Thin Solid Films, 517 (2009) 4835-4844. DOI: 10.1016/j.tsf.2009.03.018
[39] J.W. Harding, I.N. Sneddon, Mathematical Proceedings of the Cambridge Philosophical Society, 41 (2008) 16-26.DOI: 10.1017/s0305004100022325
[40] D.S. Balint, V.S. Deshpande, A. Needleman, E. Van der Giessen, J Mech Phys Solids, 54 (2006) 2281-2303. DOI: 10.1016/j.jmps.2006.07.004
[41] G.Z. Voyiadjis, M. Yaghoobi, Crystals, 7 (2017).ARTN 32110.3390/cryst7100321
[42] G.M. Pharr, E.G. Herbert, Y.F. Gao, Annual Review of Materials Research, Vol 40, 40 (2010) 271-292. DOI: 10.1146/annurev-matsci-070909-104456
[43] A. Widjaja, E. Van der Giessen, A. Needleman, Mat Sci Eng a-Struct, 400 (2005) 456-459. DOI: 10.1016/j.msea.2005.01.074
[44] H. Kreuzer, R. Pippan, Computational Mechanics, 33 (2004) 292-298
[45] R. Saha, W.D. Nix, Mat Sci Eng a-Struct, 319 (2001) 898-901. DOI: 10.1016/S0921-5093(01)01076-0
[46] R. Saha, Z.Y. Xue, Y. Huang, W.D. Nix, Journal of the Mechanics and Physics of Solids, 49 (2001) 1997-2014. DOI: 10.1016/S0022-5096(01)00035-7